IEEE Open Journal of Antennas and Propagation

A Low-RCS, High-Gain and Polarization-Insensitive FP Antenna Combing Frequency Selective Rasorber and Metasurface

Shaojie Wang[1], He-Xiu Xu[1] (Senior Member, IEEE), Mingzhao Wang[2] AND Shiwei Tang[3]

[1] Air and Missile Defense College, Air Force Engineering University, Xi'an 710051, China
[2] PLA of 93154, Jiuquan 735000, China
[3] School of Physical Science and Technology, Ningbo University, Ningbo 315211, China

CORRESPONDING AUTHOR: H-X Xu (e-mail: hxxuellen@gmail.com).

ABSTRACT A novel method to engineer high-gain and polarization-insensitive Fabry-Perot (FP) antenna with low scattering is presented by combining a polarization-insensitive broadband frequency selective rasorber with partially reflective surface (FSRP) and a reflective metasurface. The FSRP element consists of an upper indium tin oxide layer printed on polyethylene glycol terephthalate substrate, a metallic loop, and a metallic patch in the middle and bottom layer, respectively, which is designed to absorb most of out-of-band incidence while achieving in-band reflection. The bottom metallic patch is a partially reflected surface which is utilized to construct an FP resonant cavity with the reflective metasurface to ensure in-band radiation. The excellent performance of proposed FP antenna is demonstrated by simulations and measurements, revealing that the antenna exhibits an in-band peak measured gain of 21.8 dBiC at 12 GHz. Besides, a significant out-of-band scattering reduction is achieved within 9.9-11.3 GHz and 13.3-20 GHz under normal detection. Our paradigm setups a new avenue for low radar cross section of a high-gain antenna, promising great potential in practical applications.

INDEX TERMS Radar Cross Section, High-Gain, Frequency Selective Rasorber, FP Antenna

I. INTRODUCTION

Antenna, as the core of wireless communication systems, is rapidly developed in the past decades. However, as a strong scattering source, the antenna would contribute considerably to the overall radar cross section (RCS) of the entire system [1]. It is imperative to achieve an effective way to balance the contradiction between antenna radiation and scattering. Recently, metasurfaces have attracted enormously interest due to unique electromagnetic (EM) properties that are not normally found in nature materials [2]-[9]. And it is considered as an effective way to solve above contradiction.

To date, some architectures have been widely applied for antenna design based on EM band-gap (EBG) [10] and frequency selective surface (FSS) [11]. Therein, EBG structure achieves low RCS out of or in the operating band by absorbing EM waves, while FSS achieves this target by transmitting out-of-band signature. However, these methods are unable to simultaneously improve radiation and suppress scattering of the antenna, which is of great application value in the field of weaponry and national defense.

As a typical artificial reflectarray, the Fabry-Perot (FP) antenna has been proposed to achieve high radiation by constructing an FP resonant cavity with partially reflecting surface (PRS) and reflected ground and differs from Cassegrain antenna in obtaining an inherent high gain with better compactness [12]-[14]. Many stealth FP antennas have been reported so far [15]-[26]. Some are designed to absorb incident EM wave by using amplitude-modulated metasurfaces constructed from lossy materials, such as lumped resistors [15]-[17]. However, the absorption performance located at the operating band would deteriorate the gain to some extent in Ref. [16]. Besides, it is incompatible with high integration due to utilized lossy lumped resistors. Others are engineered to achieve low RCS by using phase-modulated metasurfaces, such as random surfaces and polarization conversion surfaces [18]-[26]. In Ref. [25], the FP antenna designed using a checkerboard distribution surface achieves low scattering and high gain. However, the antenna operates in single polarization and thus would limit its application. Therefore, it is of high value to design an FP antenna for real-world applications

with simple structure, excellent radiation, and polarization-insensitive stealth performance.

Recently, a rasorber has attracted broad interest from researchers in both physics and engineering communities [27]-[29]. It manifests different EM behaviors from traditional FSS, which presents a reflection band with two-edged absorption bands. Here, inspired by rasorber, it is possible to align the operation band of FP antenna within the reflection region, which avoids the degradation of in-band radiation while simultaneously achieves the reduction of out-of-band RCS in broadband. However, to the best of our knowledge, the low RCS FP antenna based on rasorber has yet been rarely reported. To fill the gap, here a novel FP antenna with wideband low RCS and high gain is firstly proposed by combining frequency selective rasorber with PRS (FSRP) and reflective metasurface. In addition, the antenna is polarization insensitive and highly integrated due to simple and symmetrical structure of the adopted meta-atom.

II. ANTENNA TOPOLOGY AND DESIGN

A. Fundamental Principal

As shown in Fig. 1, the proposed FP antenna is composed of an FSRP, a reflective metasurface, and a feed source. The FSRP achieves small in-band transmission at f_0 and two high out-of-band absorption bands at f_0-Δf_1 and f_0+Δf_2. The reflective metasurface has been used to provide an arbitrary constant phase for modulating the height H of air cavity, instead of the conventional metallic ground which has a constant reflective phase of 180°. The feed source is located at the heart of reflective metasurface to excite the entire antenna system. The resonance condition can be described as

$$\varphi_1 + \varphi_2 - 2\pi/\lambda \times 2H = -2N\pi \quad N = 1, 2, 3\cdots \qquad (1)$$

Here, φ_1 and φ_2 are reflection phases of the PRS and reflective metasurface, respectively. λ is the wavelength at the working frequency f_0 and N represents the resonance mode number.

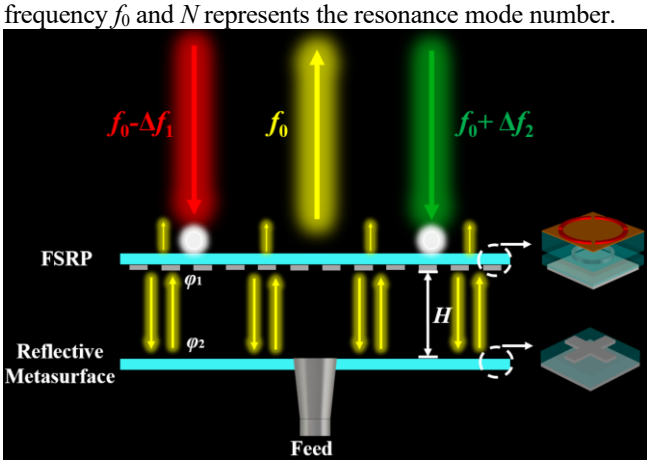

FIGURE 1. Schematic illustration of FP antenna with low RCS and high gain.

B. DESIGN OF FSRP

The key to an FSRP design lies in an effective integration of out-of-band absorption and in-band high reflection and low transmission. To address this key, an FSRP paradigm is smartly designed, as shown in Fig. 2. The top layer is a symmetrical four-open annular indium tin oxide (ITO) etched on polyethylene glycol terephthalate (PET) substrate (ε=3, tangent loss tan θ=0.003 and thickness=0.1 mm). The outer and inner radii are R_1=4.8 mm and R_2=4.2 mm and the opening width is a=0.5 mm. Although the lossy printing materials conductive ink can be utilized instead of ITO film, its manufacture is limited by high temperature or vacuum and requires surface treatment in film forming [30]. The middle layer is a metallic loop with a width of b = 0.1 mm and an inner radius of R_3 = 2.5 mm. The bottom layer is a square patch with a width of c=9.8 mm, which is used as the PRS. The dielectric spacers are two F4B substrates with a dielectric constant of 2.65 and two thicknesses of h_1=2 mm and h_2=1 mm. The period of meta-atom is P=10 mm which is targeted to the operating frequency.

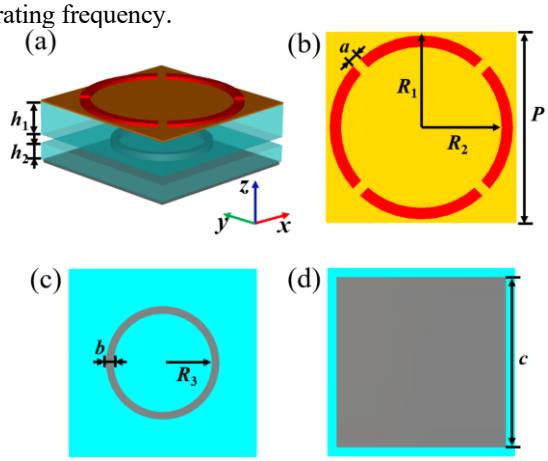

FIGURE 2. Configuration and geometric parameters of the meta-atom. (a) The perspective meta-atom. (b) ITO layer. (c) metallic loop. (d) partially reflecting surface.

The full-wave simulation is carried out to optimize meta-atom in CST Microwave 2015. The unit cell boundary condition is set in x and y directions while open (add space) boundary condition is utilized along z direction. In simulations, the EM responses of meta-atom differ when EM wave is incident along +z and -z directions, as shown in Fig. 3. Specifically, the FSRP exhibits absorption–reflection–absorption response and an in-band reflection redshift as radius of metallic loop R_3 increases while the absorption on both sides is still maintained, as shown in Fig. 3(a). A sharp selectivity occurs at 12 GHz where the reflection coefficient rises and then falls sharply when R_3=2.5 mm. The reflection coefficient (S_{11}) is less than -10 dB within 10-11.4 GHz and 12.9-19.4 GHz. The corresponding transmission (S_{21}) is always below 0.2 in 10-19.4 GHz. Based on above results, the minimum absorption calculated as 1-S_{11}^2- S_{21}^2 is 87% (10-11.4 GHz) and 88% (12.9-19.4 GHz), respectively. Nevertheless, the meta-atom serves as the PRS when EM wave is normally incident along +z-direction. The reflection amplitude is over 0.95 from 10 to 20 GHz while the phase shows a negative gradient and is -375° at 12 GHz, as shown in Fig. 3(b).

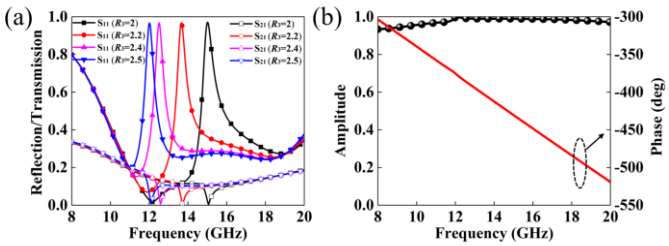

FIGURE 3. Characterizations of the FSRP. (a) Effect of different radii of metallic loop on reflection and transmission coefficients of FSRP when EM wave is incident along -z-direction. (b) Reflection amplitude and phase spectrum when EM wave is incident along +z-direction with R_3=2.5mm.

To further validate the analysis, the surface current distributions of designed FSRP are investigated at different frequencies in Fig. 4. Three frequencies are considered: the lower and higher absorption bands at 10.5 and 13 GHz, and the reflection band at 12 GHz. It is observed that the strong induced currents are generated on the four-open annular ITO layer at 10.5 and 13 GHz. The incident EM wave is absorbed due to ohmic losses. On the contrary, the metallic loop in the middle layer is excited at 12 GHz, while no significant current is observed in the ITO layer. The excited metallic loop acts as a perfect reflector, short-circuiting the ITO layer and achieving efficient reflection.

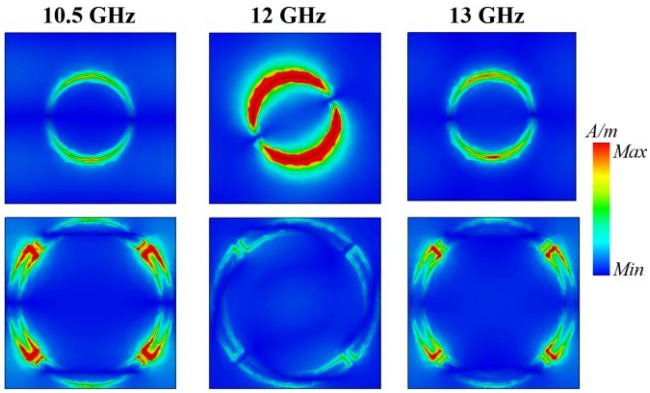

FIGURE 4. Simulated surface current distributions on different layers of FSRP at 10.5, 12 and 13 GHz.

To elucidate the absorption and reflection mechanisms, Fig. 5 illustrates the equivalent circuit model of FSRP based on the surface current distributions shown in Fig. 4. The equivalent impedance *Zs* of metallic loop is expressed as follows

$$Z_s = j\omega L_s - \frac{j}{\omega C_s} = j\omega L_s\left(1-\frac{1}{\omega^2 L_s C_s}\right) \tag{2}$$

The equivalent impedance Z_p of ITO is approximated by the following equation

$$Z_p = R + j\omega L - \frac{1}{j\omega C} \tag{3}$$

The input impedance Z_{in} of FSRP is expressed as

$$Z_{in} = \frac{1}{\frac{1}{Z_p}+\frac{1}{Z_d}+\frac{1}{Z_s}} = \frac{Z_p \times Z_d \times Z_s}{Z_p Z_d + Z_p Z_s + Z_d Z_s} \tag{4}$$

When the frequency of EM wave is aligned with the resonance of the metallic loop, $f_0=1/2\pi\sqrt{L_s C_s}$, Z_s and Z_{in} are approximately zero and the incident EM wave is reflected. While $Z_{in}\neq 0$, Z_p and Z_d play an important role in introducing resistive loss in circuit model at other frequencies beyond f_0, enabling incident EM wave to be efficiently absorbed. The parametric values of each component in the equivalent circuit can be retrieved by the fitting technique in ADS to match reflection and transmission coefficients calculated from full-wave simulation in CST.

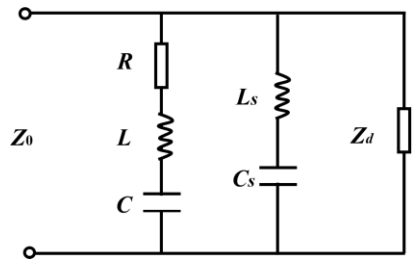

FIGURE 5. Equivalent circuit model of FSRP. *R*, *L*, and *C* denote the equivalent resistance, inductance, and capacitance of ITO, respectively. L_s and C_s are modeled as the equivalent inductance and capacitance of metallic loop. Z_0 and Z_d represent equivalent impedance of air and dielectric medium.

C. DESIGN OF REFLECTIVE METASURFACE

To satisfy the in-band FP resonance condition and reduce the cavity height, the reflective metasurface is designed to provide a flexible phase by etching a cross-shaped metal on the grounded F4B substrate with a thickness (h_3) of 2 mm (λ/12.5 at 12 GHz), as shown in Fig. 6(a). The parameters are optimized as d=2 mm and e=7.8 mm. Fig. 6(b) exhibits the reflection amplitude and phase of meta-atom simulated under normal plane waves incidence. It can be obviously seen that the reflection phase is -368° at 12 GHz. Besides, the meta-atom is insensitive to polarization due to its fourfold rotational symmetry.

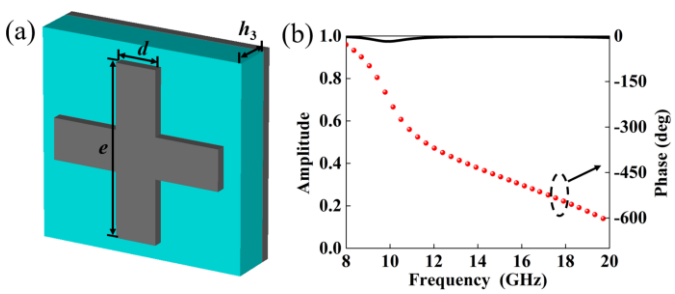

FIGURE 6. Structure and EM characteristics of the meta-atom for reflective metas-atom. (a) Geometric layout. (b) Amplitude and phase responses when EM wave is normally incident.

To determine the final meta-atom layout and indicate polarization insensitive performance, we assemble the FSRP shown in the inset of Fig. 1 and reflective metasurface shown in Fig. 6(a) to construct the whole meta-atom of FP antenna, see Fig. 7(a). The theoretical calculation referred to (1) shows that the height of the air cavity is 11.7 mm. As shown in Fig. 7 (b), the whole meta-atom exhibits similar EM response to incident waves of arbitrary polarization states. The reflection coefficient of meta-atom is still less than -10 dB within 10.1-11.9 GHz and 13.7-19.4 GHz. Moreover, the resonance of the whole meta-atom is slightly shifted to higher frequency

compared to that of individual FSRP, since the FSRP and bottom reflective metasurface are individually designed.

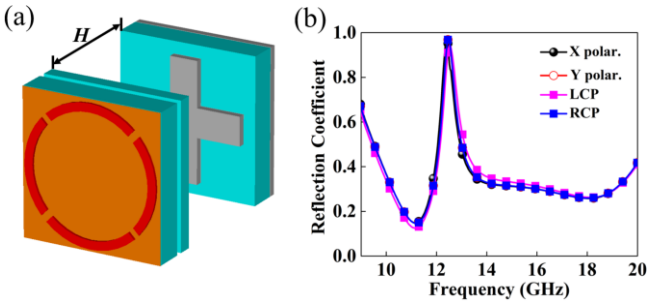

FIGURE 7. Structure and EM characteristics of the whole basic meta-atom for FP antenna. (a) Geometric layout. (b) Simulated reflection coefficient under x-polarized, y-polarized, left-handed circularly polarized (LCP) and right-handed circularly polarized (RCP) waves.

III. ANTENNA PERFORMANCE

Figs. 8(a) and 8(b) depict the layout and fabrication prototype of proposed FP antenna. An LCP helical antenna with a radius of 10 mm is located in the central of reflective metasurface to excite the entire FP antenna system. Four foam blocks are used to support two substrates, as shown in Fig 8(b). Fig. 8(c) illustrates the experimental setup for radiation performance. The FP antenna and receiver are placed on two foam cylinders. By rotating the foam cylinder on which the FP antenna is placed, the far-field radiation performance can be accurately recorded. Furthermore, the whole experiment is done in anechoic chamber to decrease influence of surrounding environment.

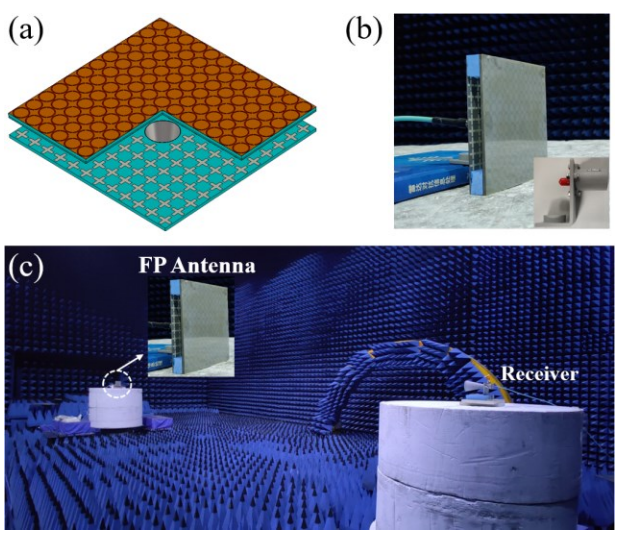

FIGURE 8. Layout and measurement setup of the FP antenna. (a) Perspective view. (b) Photograph of the fabricated sample. The inset of (b) shows the feed source. (c) Experimental setup.

A. RADIATION PERFORMANCE

In Fig. 9(a), the proposed FP antenna exhibits a 3 dB axial ratio (AR) from 11 to 13 GHz, with a minimum AR of 0.6 dB at 11.9 GHz. Fig. 9(b) shows the simulated and measured gain of the FP antenna, which reaches a maximum of 21.8 dBiC at 12 GHz. Nevertheless, the antenna gains decrease rapidly out of band where the FP resonance condition is not satisfied. The maximum aperture efficiency is calculated to be 52.3%, which is calculated by using the following equation $\eta=G\lambda^2/4\pi S$, where G is the gain of FP antenna and S represents the physical area. The measured 3 dB gain bandwidth is 11.8-12.2 GHz with a fractional bandwidth of 3.3%. Despite above good performances, there are still slight discrepancies between simulated and measured gains especially out of the operation band, which are mainly caused by tolerances inherent in fabrications and experiments.

Figs. 9(c) and (d) show the simulated and measured 2-D far-field radiation properties in xoz-and yoz-planes with different polarizations. It can be clearly seen that the FP antenna achieves high gain and polarization purity for primary polarization (LCP) component while weak radiation for cross-polarization (RCP) one at designed band. Meanwhile, the side lobe of less than -10 dB can be obtained. The antenna also possesses a 3 dB beamwidth of only 11° in xoz-and yoz-planes, which proves that the antenna radiates a highly directional beam.

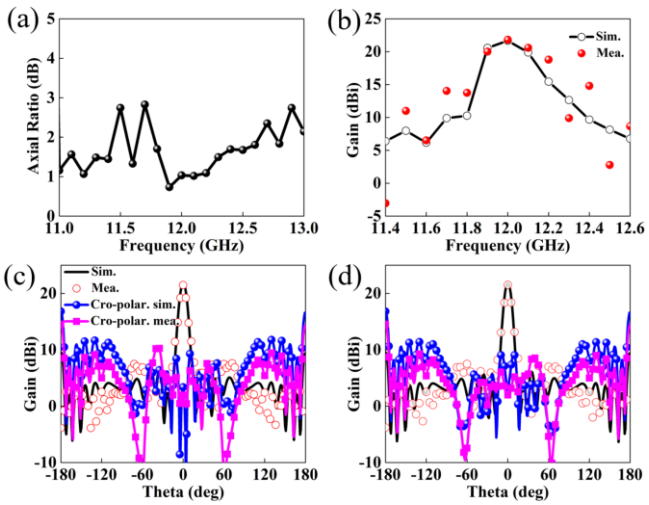

FIGURE 9. Radiation performance of the FP antennas excited by an LCP helical antenna. **(a) Simulated AR. (b) Simulated and measured (b) gain and far-field radiation patterns on (c) xoz and (d) yoz-planes at operating frequency 12 GHz.**

Moreover, we found that the maximum gain (21.8 dBiC) is achieved at 12 GHz in simulations when the height of air cavity is 12.8 mm instead of the theoretically calculated 11.7 mm. The reason for this tolerance can be interpreted as that the simulated reflection phases are not exactly the same in above two cases, which may result in the discrepancy. In full-wave simulations, the meta-atoms are impinged by ideal plane wave, while the whole FP antenna is excited by a spherical wave of a helical antenna.

B. SCATTERING PERFORMANCE

The experimental setup for far-field scattering characteristics of proposed FP antenna is shown in Fig. 10(a). Two dual CP horns set at the same horizontal plane as the FP antenna are used to transmit and receive EM waves and are connected to the AV3672B Agilent Vector Network Analyzer to record the

static EM signals. The distance between the FP antenna and two dual CP horns is arranged to more than D^2/λ to eliminate the near-field influence, where D is the diameter of CP horn's aperture. To reduce system tolerances and effect of the experimental environment, the Vector Network Analyzer is calibrated and a time domain gate method is utilized. Due to limitations of available horns in use, we only measured scattering characteristics from 8 to 18 GHz.

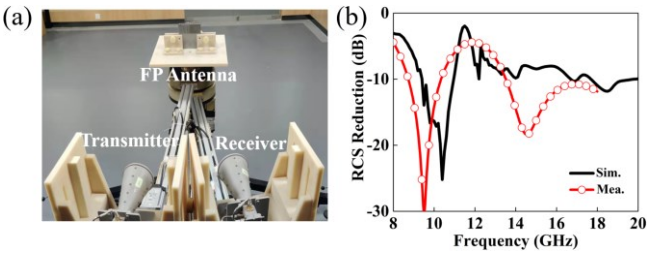

FIGURE 10. Measurement setup and scattering performance of the FP antenna. (a) Experimental setup of far-field scattering. (b) Simulated and measured RCS reduction.

The backward RCS reduction of FP antenna compared to a metal plate of the same size is presented in Fig. 10(b). In simulations, the FP antenna achieves more than 10 dB RCS reduction from 9.9 to 11.3 GHz (13.2%) and more than 8 dB RCS reduction from 13.3 to 20 GHz (40.2%). There are some discrepancies between the simulated and measured results, yet they are generally in agreement. Specifically, the resonance moves towards lower frequencies, and is significantly enhanced at higher frequencies. The discrepancies are mainly caused by the inaccurate fabrication between the FSRP and reflective metasurface. What's more, according to reciprocity principle, the antenna could receive EM wave at the operating band. Therefore, our proposed FP antenna intrinsically exhibits an inherent low scattering at 12 GHz.

Finally, Table I compares the performance of our design with that of previous works. It can be highlighted that our FP antenna exhibits full polarization behavior while achieves superior advantages of good aperture efficiency, broadband RCS reduction and high gain.

Table I. Comparisons of performance between this work and available FP antennas.

Refs.	Band	Pol.	Gain (dBiC)	Aperture efficiency	RCS (GHz)	Area(λ^2)	Profile
[16]	X	LP	18.4	40.2%	8-17	3.7×3.7	0.42λ
[18]	X	LP	7		9-20	1.2×1.2	0.54λ
[20]	X	CP	3.2	11.6%	4-13	1.2×1.2	
[21]	X	LP	19.8	55.5%	8-12	3.7×3.7	
[22]	X	LP	4.9		8-18	2.2×2.2	
[24]	X	LP	17.1		8.6-14	2.8×2.8	
[25]	C	LP	12	11.7%	4-13	2.7×2.7	0.33λ
[26]	X	LP	16.6	51%	8-19	2.6×2.0	0.9λ
This work	X	All	21.8	52.3%	9.9-11.3, 13.3-20	4.8×4.8	0.51λ

IV. CONCLUSION

A novel strategy for low-RCS, high-gain and polarization-insensitive FP antenna is proposed by smartly combining a FSRP and a reflective metasurface. For verification, an FP antenna excited by a LCP planar helical antenna is numerically studied, fabricated, and experimentally measured. Numerical and experimental results coincide well and show that the antenna achieves high gain of 21.8 dBiC at 12 GHz and broadband RCS reduction within 9.9-11.3 GHz and 13.3-20 GHz. The 3 dB AR is achieved within 11-13 GHz and the minimum AR is 0.6 dB at 11.9 GHz. Furthermore, according to reciprocity theory, the antenna also exhibits low scattering characteristics at the operation band. Due to the above advantages, we believe that the proposed FP antenna will find potential applications in communication and stealth discipline for complex EM environments.

ACKNOWLEDGMENT

This work is supported by the National Natural Science Foundation of China under Grant No. 62171459, National Defense Foundation of China under Grant No. 2019-JCJQ-JJ-081, Key Program of Natural Science Foundation of Shaanxi Province under Grant No. 2020JZ-33, Natural Science Foundation of Ningbo under Grant No. 2021J073 and the Special Talents Support Program of Shaanxi Province for Young Top Talents.

REFERENCES

[1] Y. Fan, J. Wang, Y. Li, J. Zhang, Y. Han, and S. Qu, "Low-RCS and high-gain circularly polarized metasurface antenna," *IEEE Trans. Antennas Propag*., vol. 67, no. 12, pp. 7197-7203, Dec. 2019.

[2] H.-X. Xu, H. Liu, X. Ling, Y. Sun, and F. Yuan, "Broadband vortex beam generation using multimode Pancharatnam-Berry metasurface," *IEEE Trans. Antennas Propag.*, vol. 65, no. 12, pp. 7378-7382, Oct. 2017.

[3] R. S. Malfajani and Z. Atlasbaf, "Design and implementation of a dual-band single layer reflectarray in X and K bands," *IEEE Trans. Antennas Propag*., vol. 62, no. 8, pp. 4425-4431, Aug. 2014.

[4] H.-X. Xu, T. Cai, Y.-Q. Zhuang, Q. Peng, G.-M. Wang, and J.-G. Liang, "Dual-mode transmissive metasurface and its applications in multibeam transmitarray," *IEEE Trans. Antennas Propag.*, vol. 65, no. 4, pp. 1797-1806, Feb. 2017.

[5] E. Erfani, M. Niroo-Jazi, and S. Tatu, "A high-gain broadband gradient refractive index metasurface lens antenna," *IEEE Trans. Antennas. Propag.*, vol. 64, no. 5, pp. 1968-1973, May 2016.

[6] H.-X Xu, M. Wang, G. Hu, et al., "Adaptable invisibility management using kirigami-inspired transformable metamaterials," *Research*, 9806789, 1034-1044, 2021.

[7] T. Tian, X. Huang, Y. Xu, P. Liu, C. Liu, N. Hu, J. Zhang, and Z. Wu, "A wideband energy selective surface with quasi-elliptic bandpass response and high-power microwave shielding," *IEEE Transactions on Electromagnetic Compatibility*, 3325438, 2023.

[8] H.-X. Xu et al., "Multifunctional microstrip array combining a linear polarizer and focusing metasurface," *IEEE Trans. Antennas Propag*., vol. 64, no. 8, pp. 3676-3682, Aug. 2016.

[9] Y. Liu, S. Gu, C. Luo, and X. Zhao, "Ultra-thin broadband metamaterial absorber," *Appl. Phys. A, Solids Surf.*, vol. 108, no. 1, pp. 19-24, 2012.

[10] Y. Jia, Y. Liu, H. Wang, K. Li, and S. Gong, "Low-RCS, high-gain, and wideband mushroom antenna," *IEEE Antennas Wirel. Propag. Lett.*, vol. 14, pp. 277-280, Feb. 2015.

[11] S. Genovesi, F. Costa, and A. Monorchio, "Low-profile array with reduced radar cross section by using hybrid frequency selective surfaces," *IEEE Trans. Antennas Propag.*, vol. 60, no. 5, pp. 2327-2335, May 2012.

[12] W.-L. Guo et al., "Broadband polarization-conversion metasurface for a Cassegrain antenna with high polarization purity," *Phys Rev Appl*., vol. 12, no. 1, Jul. 2019.

[13] G.-P. Gao, C. Yang, B. Hu, S.-F. Wang, and R.-F. Zhang, "Design of a high-gain and low-profile quasi-Cassegrain antenna based on metasurfaces," *IEEE Antennas Wirel. Propag. Lett.*, vol. 17, no. 8, pp. 1435-1439, Aug. 2018.

[14] S. Wang, H-X. Xu, M. Wang, C. Wang, Y. Wang, and X. Ling, "A Low-RCS and High-Gain Planar Circularly Polarized Cassegrain Meta-Antenna," *IEEE Trans. Antennas Propag.*, vol. 70, no. 7, pp. 5278-5287, Jul. 2022.

[15] C. Huang, W. B. Pan, X. L. Ma, and X. G. Luo, "A frequency reconfigurable directive antenna with wideband low-RCS property," *IEEE Trans. Antennas Propag.*, vol. 64, no. 3, pp. 1173-1178, Mar. 2016.

[16] H. Jiang, Z. H. Xue, W. M. Li, W. Ren, and M. Cao, "Low-RCS high-gain partially reflecting surface antenna with metamaterial ground plane," *IEEE Trans. Antennas Propag.*, vol. 64, no. 9, pp. 4127-4132, Sep. 2016.

[17] W. Pan, C. Huang, P. Chen, X. Ma, C. Hu, and X. Luo, "A low-RCS and high-gain partially reflecting surface antenna," *IEEE Trans. Antennas Propag.*, vol. 62, no. 2, pp. 945-949, Feb. 2014.

[18] M. Long, W. Jiang, and S. Gong, "Wideband RCS reduction using polarization conversion metasurface and partially reflecting surface," *IEEE Antennas Wirel. Propag. Lett.*, vol. 16, pp. 2534-2537, 2017.

[19] S. M. A. Momeni Hasan Abadi and N. Behdad, "Wideband Linear-to-Circular Polarization Converters Based on Miniaturized-Element Frequency Selective Surfaces," *IEEE Trans. Antennas Propag.*, vol. 64, no. 2, pp. 525-534, Feb. 2016.

[20] J. Ren, W. Jiang, K. Zhang, et al. "A High-gain circularly polarized Fabry-Perot antenna with wideband low-RCS property," *IEEE Antennas Wirel. Propag. Lett.*, vol. 17, no. 5, pp. 853-856, May. 2018.

[21] L. Zhang et al., "Realization of low scattering for a high-gain Fabry-Perot antenna using coding metasurface," *IEEE Trans. Antennas Propag.*, vol. 65, no. 7, pp. 3374-3383, July 2017.

[22] Y. Zheng et al., "Wideband gain enhancement and RCS reduction of Fabry-Perot resonator antenna with chessboard arranged metamaterial superstrate," *IEEE Trans. Antennas Propag.*, vol. 66, no. 2, 410 pp. 590-598, Feb. 2018.

[23] K. Li, Y. Liu, Y. Jia, and Y. J. Guo, "A Circularly Polarized High-Gain Antenna with Low RCS Over a Wideband Using Chessboard Polarization Conversion Metasurfaces," *IEEE Trans. Antennas Propag.*, vol. 65, no. 8, pp. 4288-4292, Aug. 2017.

[24] Z. Liu, S. Liu, X. Zhao, et al., "Wideband gain enhancement and RCS reduction of Fabry-Perot antenna using hybrid reflection method," *IEEE Trans. Antennas Propag.*, vol. 68, no. 9, pp. 6497-6505, Sept. 2020.

[25] H. Umair et al., "Fabry-Perot antenna employing artificial magnetic conductors and phase gradient metasurface for wideband monostatic RCS reduction and high gain tilted beam radiation," *IEEE Access*, vol. 9, pp. 66607-66625, 2021.

[26] X. Liu, Z. Yan, E. Wang, T. Zhang, and F. Fan, "Magnetoelectric dipole-fed Fabry–Perot antenna with wideband RCS reduction based on multilayer metasurface," *IEEE Antennas and Wireless Propagation Letters*, vol. 20, no. 7, pp. 1342-1346, July 2021.

[27] W. Wu, K. Cui, H. Lu, et al., "A measured rasorber with two absorptive bands," *Radioengineering*, vol. 26, no. 4, pp. 979-983, Feb. 2018.

[28] Y. Han, W. Che, X. Xiu, W. Yang, and C. Christopoulos, "Switchable low-profile broadband frequency-selective rasorber/absorber based on slot arrays," *IEEE Trans. Antenna Propag.*, vol. 65, no. 12, pp. 6998-7008, Dec. 2017.

[29] A. Motevasselian and B. L. G. Jonsson, "Design of a wideband rasorber with a polarisation sensitive transparent window," *IET Microw. Antenna Propag.*, vol. 6, no. 7, pp. 747-755, May 2012.

[30] E. Dimitriou and N. Michailidis, "Printable conductive inks used for the fabrication of electronics: an overview", *Nanotechnology* 32 502009, 2021.